Evaluation of PPP-RTK based on BDS-3/BDS-2/GPS observations: a case study in Europe

Zhao Li[1]·Wu Chen[1]·Rengui Ruan[2]·Xuexi Liu[3]

Zhao Li

zhao.mm.li@polyu.edu.hk

1 Department of Land Surveying and Geo-Informatics, The Hong Kong Polytechnic University, 181 Chatham Road South, Hung Hom, Kowloon 999077, Hong Kong, People's Republic of China

2 Xi'an Research Institute of Surveying and Mapping, 1 Middle Yanta Road, Xi'an 710054, People's Republic of China

3 School of Geodesy and Geomatics, Wuhan University, 129 Luoyu Road, Wuhan 430079, People's Republic of China

Abstract The Chinese BeiDou Navigation Satellite System (BDS) transited from regional (Asia-Pacific) to global on December 28, 2018. In this study, the performance of PPP-RTK based on BDS-3/BDS-2/GPS observations is analyzed by utilizing the observations in Europe during a calm ionospheric disturbance period with Kp-index ranging from 0o to 2-. Satellite clock offsets are first estimated and then fixed to determine the uncalibrated phase delays (UPDs) and the ionospheric/tropospheric information from the reference network. Real-time PPP and PPP AR based on raw observations are conducted at the user, in which atmospheric constraints are imported as virtual observations if available. Analysis results based on three days of observations reveal that centimeter-level positioning accuracy can be achieved based on GPS, BDS or GPS+BDS observations, and the performance can be further improved by realizing PPP AR. The satellite-differenced ionospheric and tropospheric information can be predicted for the users with an accuracy of 24.6 mm

and 5.6 mm respectively. Augmented by the predicted atmospheric information, PPP-RTK can be realized based on GPS or BDS only observations, and the average number of epochs required for ambiguity fixing is 1.5 and 1.6 respectively. The RMS values of the positioning errors of the north, east, up components based on GPS only observations are 8.0, 4.7, and 19.7 mm, while 9.8, 7.3, 29.7 mm respectively based on BDS only observations. Utilizing GPS and BDS observations together, the average number of epochs required decreases to 1.2, and the positioning errors become 5.6, 3.5, and 23.3 mm for the north, east, and up components, respectively. All these results suggest that BDS can provide high accuracy positioning services independently for users in Europe. Although a small decrease in the positioning accuracy of the up component, which might be attributed to in-appropriate weighting strategy between satellite systems and requires further researches in the future, the additional BDS observations can improve the performance in the time to the first fixed solution and the positioning accuracies with respect to GPS only positioning. The performance of PPP-RTK based on BDS-3/BDS-2/GPS observations during medium and high ionospheric disturbance periods will also be conducted in the future to fully evaluate the effects of additional BDS-3 observations in high-accuracy GNSS applications.

Keywords

BDS-3, GPS, Precise Point Positioning (PPP), ambiguity resolution (AR), atmospheric information

Introduction

The development of the Chinese BeiDou Navigation Satellite System (BDS) can be divided into three steps: the experiment system (BDS-1), the regional system (BDS-2), and the global system (BDS-3). After the success of BDS-1 and BDS-2, construction of the global system began in 2015. A demonstration system with five satellites, also called BDS-3e, had been launched between 2015 and 2016 to verify the design of the BDS-3 fully, and the first two BDS-3 satellites were launched on November 5, 2017 (Yang et al. 2018). The BDS system is expected to consist of 35 satellites by 2020 (Yang et al. 2017).

Following the analysis of BDS-2, including the observation quality (Wanninger and Beer 2015), satellite orbit and clock determination (Steigenberger et al. 2013; Tegedor et al. 2014), relative and absolute positioning (Montenbruck et al. 2013; Odolinski et al. 2013; Yang et al. 2014; Li et al. 2015; Zhang and He 2016; Kamil et al. 2018), various studies concerning the performance of BDS-3 have been conducted along with the system development. Analysis found that the satellite-induced code biases that existed in the BDS-2 observations are not present for the BDS-3e satellites (Zhang et al. 2017; Xu et al. 2018). The phase multipath, as well as the code and phase noises of the BDS-3e satellites, are comparable to that GPS Block IIF and Galileo (Zhang et al. 2017). This provide a very good basis for BDS-3 orbit and clock determination. Evaluated by orbit overlap comparisons and SLR validations, researchers found that the orbit accuracies of BDS-3e and BDS-3 were comparable to BDS-2 satellites (Li et al. 2019; Xu et al. 2018), while the clock accuracy and stabilities of onboard clocks were slightly better than that of the BDS-2 MEO satellites (Yan et al. 2019). With respect to the performance of BDS-3 in the field of precise positioning, Zhang et al. (2017, 2018) confirmed that the performance in ambiguity resolution (AR) and real-time kinematic (RTK) positioning could be improved by the additional BDS-3e observations, indicating that the BDS-3e satellites could contribute to precise relative positioning. By incorporating BDS-2 with BDS-3e

observations, the convergence of Precise Point Positioning (PPP) could also be effectively improved (Xu et al. 2018; Zhang et al. 2018; Zhao et al. 2018).

On December 27, 2018, the BDS system was announced to provide global services for users. There are in total 34 BDS-2/BDS-3e/BDS-3 satellites in the constellation, including 5 Geostationary Earth Orbit (GEO), 8 Inclined Geosynchronous Satellite Orbit (IGSO), and 21 Medium Earth Orbit (MEO) (http://mgex.igs.org/IGS_MGEX_Status_BDS.php). However, the existing analysis related to the performance of BDS positioning is mostly on BDS-2 observations due to the fewer BDS-3/BDS-3e satellites in orbit (Xu et al. 2018; Yan et al. 2019; Zhang et al. 2017; Zhang et al. 2018). In addition, previous precise positioning based on BDS observations is only analyzed for those users in Asia-Pacific regions, where the operational services are provided by the BDS-2 system. These results cannot well represent the capability of BDS-3 in providing high-precision services for global users. With more BDS-3/BDS-3e satellites in orbit, further analysis of accurate user positioning using observations from BDS-3/BDS-2 alone or together with other Global Navigation Satellite System (GNSS) for those users outside the Asia-Pacific regions are required and important for the promotion of its wide applications in other regions or globally.

The PPP method has already been widely used in various fields, such as timing, meteorology, and Low Earth Orbit (LEO) satellite orbit determination (de Haan et al. 2009; Defraigne et al. 2015; Bock et al. 2009), and PPP ambiguity resolution (AR) can improve the performance by fixing the satellite-differenced or undifferenced ambiguities to integers aided by the satellite uncalibrated phase delays (UPDs) or integer satellite clock products (Ge et al. 2008; Laurichesse et al. 2009). Furthermore, PPP-RTK realizes instantaneous or rapid PPP AR by importing the predicted atmospheric information generated from regional network stations for parameter estimation, thus can further shorten the time-to-first-fix (TTFF) in PPP AR (Li et al. 2011; Nadarajah et al. 2018; Wübbena et al. 2005; Zhang et al. 2011). Currently, PPP-RTK can achieve the performance comparable to that of network real-time kinematic (NRTK) and has become an important tool in high accuracy applications.

In this study, we realize PPP-RTK based on BDS-3/BDS-2/GPS observations and analyze its performance by utilizing the observations in Europe. The data processing strategies at the server and the user are introduced first. The observation data and models adopted in the analysis are then illustrated. In the following, the analysis results are presented in detail, and some conclusions are given last.

Data processing strategy

We first introduce the general observation model of the raw code and phase observations. After that, the data processing strategies for satellite clock offset and UPD estimation, as well as the ionospheric/tropospheric prediction at the server are explained. Finally, the algorithms in real-time (RT) PPP and PPP AR at the user are presented in detail.

General Observation Model

The observation equation of dual-frequency observations can be expressed as follows:

$$\begin{aligned}
P_{r,1}^{m,S} &= \rho_{r,1}^{m,S} + c\Delta t_r^S - c\Delta T^{m,S} + b_{r,1}^S - b_1^{m,S} + \delta I_r^{m,S} + \delta T_r^{m,S} + \Delta_{r,1}^{m,S} \\
P_{r,2}^{m,S} &= \rho_{r,2}^{m,S} + c\Delta t_r^S - c\Delta T^{m,S} + b_{r,2}^S - b_2^{m,S} + \frac{f_1^2}{f_2^2}\delta I_r^{m,S} + \delta T_r^{m,S} + \Delta_{r,2}^{m,S} \\
L_{r,1}^{m,S} &= \rho_{r,1}^{m,S} + c\Delta t_r^S - c\Delta T^{m,S} + d_{r,1}^S - d_1^{m,S} - \delta I_r^{m,S} + \delta T_r^{m,S} - \lambda_1^S N_{r,1}^{m,S} + \varepsilon_{r,1}^{m,S} \\
L_{r,2}^{m,S} &= \rho_{r,2}^{m,S} + c\Delta t_r^S - c\Delta T^{m,S} + d_{r,2}^S - d_2^{m,S} - \frac{f_1^2}{f_2^2}\delta I_r^{m,S} + \delta T_r^{m,S} - \lambda_2^S N_{r,2}^{m,S} + \varepsilon_{r,2}^{m,S}
\end{aligned} \tag{1}$$

where S represents the satellite system (GPS and BDS here), r and m denote the receiver and satellite respectively, c represents the speed of light; $P_{r,i}^{m,S}$ and $L_{r,i}^{m,S}\left(i=1,2\right)$ denote the code and phase observations at each frequency, $\mathrm{D}t_r^S$ and $\mathrm{D}T^{m,S}$ represent the clock offsets of the receiver and satellite. The symbols $b_{r,i}^S$ and $b_i^{m,S}\left(i=1,2\right)$ represent the instrumental biases of the receiver and satellite for code observations at each frequency, while $d_{r,i}^S$ and $d_i^{m,S}\left(i=1,2\right)$ denote the

corresponding biases for phase observations. $\delta I_r^{m,S}$ represents the ionospheric delay along the signal path at the first frequency, $f_i\,(i=1,2)$ denotes the frequency, $\delta T_r^{m,S}$ denotes the slant tropospheric delay. $\lambda_i^S\,(i=1,2)$ represents the wavelength of the signal at each frequency, and $N_{r,i}^{m,S}$ denotes the ambiguity. $\mathrm{D}_{r,i}^{m,S}$ and $\varepsilon_{r,i}^{m,S}$ are the random noises and unmodeled errors of the code and phase observations, respectively.

Since the equations contain terms that cannot be estimated individually, a re-parameterization is necessary before estimation. According to the IGS convention, the precise satellite and receiver clock offsets absorb the ionospheric-free combination of satellite and receiver biases of the code observations, respectively (Kouba 2009). Therefore, the re-parameterized estimable parameters of the model can be expressed as follows:

$$
\begin{aligned}
&\Delta t_r' = \Delta t_r + \frac{f_1^2 b_{r,1}^S - f_2^2 b_{r,2}^S}{c\left(f_1^2 - f_2^2\right)} \\
&\Delta T'^{m,S} = \Delta T^{m,S} + \frac{f_1^2 b_1^{m,S} - f_2^2 b_2^{m,S}}{c\left(f_1^2 - f_2^2\right)} \\
&I' = I - \frac{f_2^2}{f_1^2 - f_2^2}\left(b_{r,1}^S - b_{r,2}^S\right) + \frac{f_2^2}{f_1^2 - f_2^2}\left(b_1^{m,S} - b_2^{m,S}\right) \\
&\lambda_1^S N_{r,1}'^{m,S} = \lambda_1^S N_{r,1}^{m,S} + \left[\frac{\left(f_1^2 + f_2^2\right)b_{r,1}^S - 2 f_2^2 b_{r,2}^S}{f_1^2 - f_2^2} - d_{r,1}^S\right] - \left[\frac{\left(f_1^2 + f_2^2\right)b_1^{m,S} - 2 f_2^2 b_2^{m,S}}{f_1^2 - f_2^2} - d_1^{m,S}\right] \\
&\lambda_2^S N_{r,2}'^{m,S} = \lambda_2^S N_{r,2}^{m,S} + \left[\frac{2 f_1^2 b_{r,1}^S - \left(f_1^2 + f_2^2\right)b_{r,2}^S}{f_1^2 - f_2^2} - d_{r,2}^S\right] - \left[\frac{2 f_1^2 b_1^{m,S} - \left(f_1^2 + f_2^2\right)b_2^{m,S}}{f_1^2 - f_2^2} - d_2^{m,S}\right]
\end{aligned}
\tag{2}
$$

In addition, the tropospheric delay can be modeled as the sum of the hydrostatic and non-hydrostatic part, among which the hydrostatic part can be accurately modeled and corrected by the a priori model, while the non-hydrostatic part is difficult to be modeled and must be estimated as unknown parameters in precise applications. Other systematic errors, such as the solid earth tide, the ocean tide, the relativistic effects, as well as the satellite/receiver phase center offset (PCO) and phase center variation (PCV), can be corrected by the corresponding a priori models. Then, the observation equations of the raw code and phase observations become (Liu et al. 2017):

$$
\begin{aligned}
P_{r,1}^{m,S} &= \rho_{r,1}^{m,S} + c\Delta t_r'^S - c\Delta T'^{m,S} + \delta I_r'^{m,S} + m^{m,S}\delta T_{wr} + \Delta_{r,1}^{m,S} \\
P_{r,2}^{m,S} &= \rho_{r,2}^{m,S} + c\Delta t_r'^S - c\Delta T'^{m,S} + \frac{f_1^2}{f_2^2}\delta I_r'^{m,S} + m^{m,S}\delta T_{wr} + \Delta_{r,2}^{m,S} \\
L_{r,1}^{m,S} &= \rho_{r,1}^{m,S} + c\Delta t_r'^S - c\Delta T'^{m,S} - \delta I_r'^{m,S} + m^{m,S}\delta T_{wr} - \lambda_1^S N_{r,1}'^{m,S} + \varepsilon_{r,1}^{m,S} \\
L_{r,2}^{m,S} &= \rho_{r,2}^{m,S} + c\Delta t_r'^S - c\Delta T'^{m,S} - \frac{f_1^2}{f_2^2}\delta I_r'^{m,S} + m^{m,S}\delta T_{wr} - \lambda_2^S N_{r,2}'^{m,S} + \varepsilon_{r,2}^{m,S}
\end{aligned}
\tag{3}
$$

where $m^{m,S}$ represents the mapping function of the non-hydrostatic part, and δT_{wr} denotes the zenith non-hydrostatic delay (ZWD) at the station. It must be pointed out that the ambiguities in this model are float values since they absorb a combination of satellite/receiver instrumental bias for code and phase observations. Thus, ambiguity resolution can only be applied to double-differenced ambiguities. The observation model with integer ambiguities proposed by Odijk et al. (2016), which retains the integer feature of ambiguities at each frequency and which can fix the ambiguities directly to extract UPDs, is more applicable to the multi-GNSS, multi-frequency data processing, and will be imported in the future.

Real-time satellite clock offset and UPDs estimation

In RT satellite clock offset estimation, the method proposed by Ge et al. (2012) is utilized and adapted here to process the BDS-3/BDS-2/GPS observations together. We then fix the calculated satellite clock offsets, process the raw observations of all reference stations together according to (3), and calculate the float ambiguities $N_i'(i=1,2)$. We then apply double-difference ambiguity resolution based on the sequential ambiguity-fixing strategy (Dong and Bock 1989), among which only those ambiguities between satellites of the same satellite systems are attempted to be fixed. Due to the ionospheric delay, the raw ambiguities cannot be easily separated accurately. Therefore, the ambiguity resolution procedure is divided into wide-lane (WL) and narrow-lane (NL) combinations. The double-difference WL ambiguity can be calculated from the raw float ambiguities and expressed as follows:

$$\Delta\nabla N_{wl}' = \Delta\nabla N_1' - \Delta\nabla N_2' \tag{4}$$

where Δ and ∇ represent station-differencing and satellite-differencing respectively, and N_{wl}' denotes the WL ambiguity.

The double-differenced NL ambiguity is attempted to be fixed after successfully fixing the WL combination. The float value can be calculated from the raw float ambiguities and expressed as:

$$\Delta\nabla N'_{nl} = \frac{f_1\Delta\nabla N'_1 - f_2\Delta\nabla N'_2}{f_1 - f_2} - \frac{f_2}{f_1 - f_2}\Delta\nabla\tilde{N}'_{wl} \quad (5)$$

where $\Delta\nabla\tilde{N}'_{wl}$ denotes the fixed integer value of double-difference WL ambiguity.

After ambiguity resolution, the fixed ambiguities are imported as virtual observations with infinite weights in parameter estimation to generate the fixed network solution, from which the ionospheric and tropospheric information for later interpolation by the user can be obtained directly. In addition, the fractional offsets of the WL and NL combination of satellite-differenced ambiguities are considered as the corresponding UPDs between satellites for the following PPP AR at the user.

Prediction of ionospheric and tropospheric corrections

After extracting the ionospheric and tropospheric information of all reference stations, interpolation should be implemented to predict the ionospheric and tropospheric corrections for users. Until now, various interpolation methods have been proposed, such as linear combination method (LCM), linear interpolation method (LIM), and distance-based linear interpolation method (DIM). Analysis results have revealed that the performance of these methods is comparably (Dai et al. 2003). In this analysis, we select the DIM method to interpolate the atmospheric delay to the user position. Suppose that the ionospheric or tropospheric delays are $A_j\left(j = 1,2,\cdots,n\right)$ for the reference stations, and n is the number of reference stations, the interpolated ionospheric or tropospheric delay at the user position can be expressed as:

$$\tilde{A}_u = \frac{\sum_{j=1}^{n} p_j A_j}{\sum_{j=1}^{n} p_j} \quad (6)$$

where p_j represents the weighting factor of each reference station, which is inverse proportional to the distance between the reference station and the user. When predicting the ionospheric corrections, the posterior variance of interpolated results,

which equals to $[\sum_{j=1}^{n} p_j \left(A_j - \tilde{A}_u\right)^2] / [(n-1)\sum_{j=1}^{n} p_j]$, is also calculated.

Since the estimated ionospheric parameters could absorb receiver biases, which is different between stations, the ionospheric prediction is only applied in a satellite-differenced mode, to eliminate the impact of the receiver instrumental biases. In addition, only if the satellite-differenced ambiguities are successfully fixed for one station, the satellite-differenced ionospheric delay of this station will be applied for the prediction. Considering the spatial correlation of the atmospheric parameters, only those reference stations with distances to the users smaller than 200 km are selected for the prediction in this analysis.

Real-time PPP and PPP AR

At the user, we also process the raw observations directly according to (3), and the ionospheric and tropospheric constraints generated from the reference network are imported as virtual observations for parameter estimation if available:

$$\begin{aligned} \delta\tilde{I}_u'^{m_1,m_2,S} &= \delta I_u'^{m_1,S} - \delta I_u'^{m_2,S} + \sigma_I \\ \delta\tilde{T}_{wu} &= \delta T_{wu} + \sigma_T \end{aligned} \tag{7}$$

where $\delta\tilde{I}_u'^{m_1,m_2,S}$ represents the predicted ionospheric delay between satellites m_1 and m_2 at the first frequency, $\delta\tilde{T}_{wu}$ denotes the predicted ZWD. s_I and s_T are the random errors of the predicted ionospheric and tropospheric results respectively. The variance of the predicted ionospheric information is fixed to the posterior variance calculated in ionospheric prediction previously and set at least to 9 cm^2. The variance of predicted ZWD is fixed to 36 mm^2 in the data processing.

The float values of raw ambiguities and their corresponding variance matrix can then be obtained after parameter estimation. Like the data processing at the server, the WL and NL ambiguity resolution is conducted separately to realize PPP AR. We select the satellites with highest elevation as reference satellites for each satellite system, the satellite-differenced WL and NL ambiguities attempted to be fixed can be

expressed as:

$$\begin{aligned} \nabla N'_{wl} &= \nabla N'_1 - \nabla N'_2 - upd^{ij}_{wl} \\ \nabla N'_{nl} &= \frac{f_1 \nabla N'_1 - f_2 \nabla N'_2}{f_1 - f_2} - \frac{f_2}{f_1 - f_2} \nabla \tilde{N}'_{wl} - upd^{ij}_{nl} \end{aligned} \tag{8}$$

where upd^{ij}_{wl} and upd^{ij}_{nl} denote the satellite-differenced WL and NL UPDs, respectively, while $\nabla \tilde{N}'_{wl}$ represents the fixed satellite-differenced WL ambiguity. The variance matrix of the two combinations can be calculated by error propagation law.

In each step, the ambiguities are attempted to be fixed using the LAMBDA method (Teunissen 1995), and the ratio test, of which the criterion is set to 3, is applied to validate the results. In addition, a partial AR strategy is adopted in the analysis (Ge and Shi 2017). Each time when AR is failed, ambiguity candidates with the lowest precision is excluded and then AR is re-attempted. In the case that a group with more than 4 ambiguity candidates passed the test, the ambiguities are successfully fixed. Otherwise, the ambiguities are considered not resolved. When succeeded in each step, the fixed ambiguities are imported as virtual observations to update the solutions, and the final fixed PPP solutions can be obtained when both WL and NL AR are successful.

Data and models

Thirty-one European Permanent GNSS Network (EPN) stations, plotted in Fig.1, are selected. Among them, 20 stations located in Finland are equipped with Javad receivers and capable of tracking BDS-3/BDS-2/GPS satellites, while another 11 stations track only GPS satellites. The tracking network covers an area with a radius of about 2000 km, while those stations in Finland, which are capable of tracking BDS-3/BDS-2 satellites, cover an area with a radius of about 700 km. The observations of this tracking network provide a very good opportunity to evaluate the performance of PPP-RTK based on BDS-3/BDS-2/GPS observations. During the

following analysis, 30 stations (blue dots in Fig. 1) are selected as reference stations, and the remaining station (OUL2, red dot in Fig. 1) in Finland is selected as user station. At the server, the BDS-3/BDS-2/GPS observations are processed together. All 30 reference stations are applied to calculate the satellite clock offsets, while only 19 reference stations located in Finland are utilized to calculate the UPDs and atmospheric information. At the user, PPP-RTK based on observations of GPS, BDS and GPS+BDS are conducted separately for OUL2 to evaluate the performance based on observations of different satellite systems. The average and largest distance between OUL2 and all reference stations are about 729 km and 2000 km, while about 371 km and 620 km between OUL2 and those reference stations located in Finland. We use three days (December 24-26, 2018) of observations to conduct the analysis. The final Kp-index determined by GeoForschungsZentrum (GFZ), Potsdam, Germany, ranges from 0o to 2- (https://www.gfz-potsdam.de/en/kp-index/), indicating a low ionospheric disturbance during the period. The observations are processed each day in a simulated RT mode, which means only forward filtering is allowed. The convergence time required for satellite clock offset estimation is set to 30 minutes, from when the satellite correction messages can be continuously calculated unless all observations between reference stations and this satellite experience cycle slips or re-initializations. In addition, user positioning at the user is conducted since UTC 2h of each day, which means that 22 hours of positioning results are generated each day.

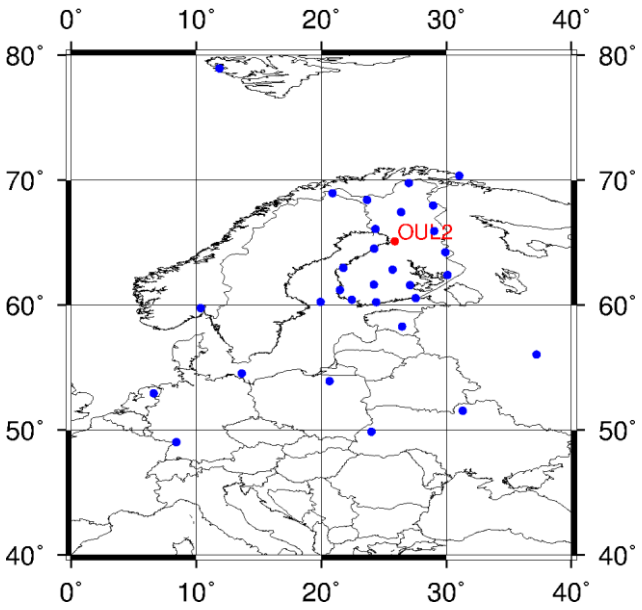

Fig. 1 Distribution of reference (blue) and user (red) stations from EPN

The final GNSS satellite orbits calculated at Xi'an Research Institute of Surveying and Mapping are used and fixed in the analysis. Station coordinates are obtained from the combined weekly EPN solution. During data processing, GPS observations of L1 and L2 frequency, together with BDS observations of B1 and B3 frequency, are processed. The PCO and PCV correction values for GPS satellites are obtained from the latest IGS14.atx antenna calibration file, while for BDS satellites, the PCO values are obtained from the manufacturers and no PCV corrections are applied. The receiver PCO and PCV values obtained from the IGS14.atx file are applied to both GPS and BDS. The elevation-dependent code biases of the BDS-2 IGSO/MEO satellites calculated by Wanninger and Beer (2015) are adopted. The elevation cut-off angle is set to 10^{o}, and an elevation-dependent weighting strategy is applied to adjust the weighting of observations at different elevations. The standard deviation (STD) of the GPS code and phase observations at the zenith direction is set to 0.3 and 0.003 m respectively (Pan et al. 2017), and equal weights are applied to BDS-3/BDS-2 observations except that the values for BDS-2 GEO satellites are set to 1.5 and 0.015 m respectively considering the lower GEO satellite orbit accuracy and uncorrected code bias variation (Lou et al. 2017). The temperature and pressure values are calculated by the Global Pressure and Temperature (GPT) model and then

297 applied to calculate the zenith hydrostatic delay (ZHD). The ZWD is modeled as a
298 random walk process, in which the noise intensity is set to $5.e-5m/\sqrt{s}$. The Global
299 Mapping Function (GMF) is applied to modeling the tropospheric delay (Boehm et al.
300 2006). All data processing in user positioning is conducted in kinematic mode, which
301 means that the station coordinates at each epoch were estimated as white noise.
302

303 **Results and analysis**

304 In order to evaluate the performance in user positioning based on different types of
305 satellite products, we first evaluate the performance of RT PPP and PPP AR based on
306 satellite clock offsets and UPDs only. The accuracies of predicted ionospheric and
307 tropospheric delays are then analyzed, and the performance of PPP-RTK based on
308 GPS, BDS, and GPS+BDS observations is compared in detail.
309

310 Performance of RT PPP and PPP AR

311 We conduct RT PPP and PPP AR to evaluate the accuracy of satellite clock offsets and
312 UPDs. The number of satellites tracked and Position Dilution of Precision (PDOP)
313 values based on observations of different satellite systems are plotted in Figure 2.
314 About 10 GPS and BDS satellites are tracked at each epoch, and the average number
315 is 9.5 and 10.4, respectively. When utilizing both GPS and BDS observations, the
316 number of satellites tracked exhibits a great increase. At least 14 satellites are tracked
317 for each epoch, and the average number is 20.0. The PDOP values based on single
318 GPS or BDS observations are smaller than 5 at most times, with an average value of
319 4.3 and 3.1, respectively. However, the values become much bigger with decreased
320 number of satellites tracked during some periods. Such situation can be eliminated by
321 utilizing observations of both systems together, in which the PDOP values are all
322 smaller than 3.0, with an average as 1.5.

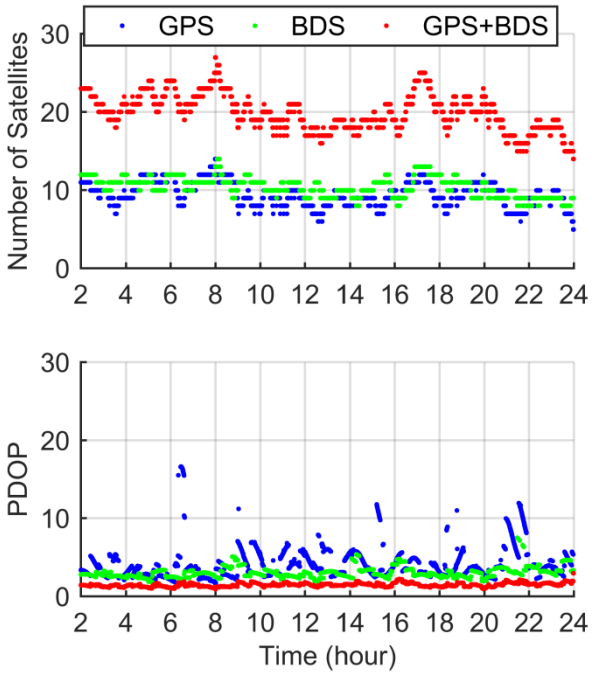

Fig. 2 Number of satellites tracked (top) and PDOP values (bottom) on Day of Year (DOY) 358, 2018

The positioning errors of the float and fixed solutions obtained from different satellite systems on DOY 358, 2018 are plotted in Fig. 3. For the float solutions (left panels), an initialization process exists under all three situations, and the positioning results based on BDS observations exhibit the slowest convergence (left-middle panel). After the initialization process, centimeter accuracy positioning results can be achieved. The positioning errors based on single BDS observations are slightly worse than that based on single GPS observations, especially for the up component, while results based on GPS+BDS observations are the most stable compared with the other two situations. With respect to the fixed solutions (right panels), sudden decrease in the positioning errors can be noticed in all three modes, which reveals the advantages of RT PPP AR in accelerating the initialization process.

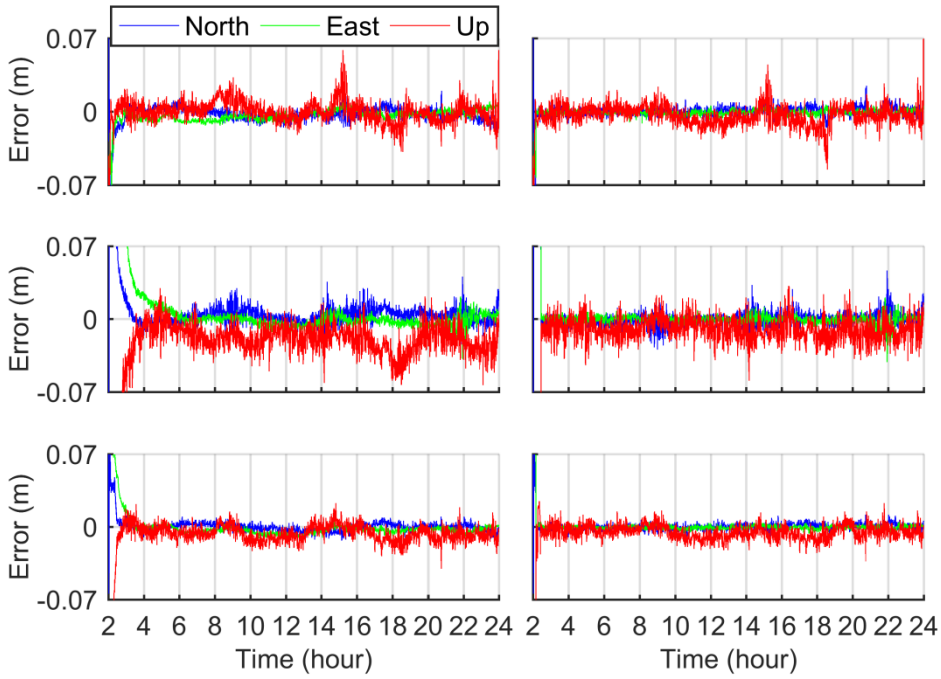

Fig. 3 Positioning errors of the float (left) and fixed (right) solutions based on GPS (top), BDS (middle), and GPS+BDS (bottom) observations

Fig. 4 shows the RMS of the positioning errors for the float and fixed solutions in different modes for all three days. Since the initialization time in RT PPP varies between days, we ignore the first two hours in all situations when evaluating the positioning accuracies to ensure that the initialization process in RT PPP has been finished and the fixed solution in PPP AR has been achieved. Thus, 20 hours of positioning results are evaluated at each day. We again find that centimeter-level accuracy positioning results can be obtained based on single or dual system observations. The positioning accuracies based on BDS observations are a little worse than that based on GPS observations, which might relate to lower satellite orbit/clock accuracy and the inaccurate observation error modeling during the data processing (Tegedor et al. 2014). As expected, the solutions based on GPS+BDS observations achieve the best performance, and the fixed solutions are more accurate than the float solutions, among which the positioning RMS of the fixed solution based on GPS+BDS observations is smaller than 10 mm in all three directions.

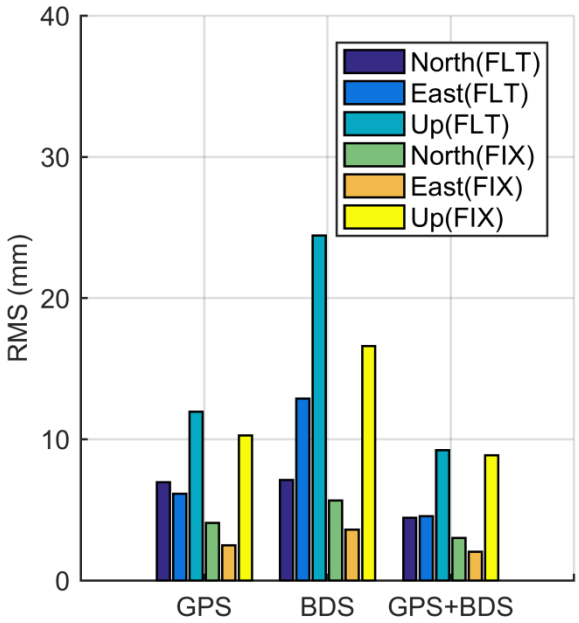

Fig. 4 RMS of the positioning errors for the float and fixed solutions, based on GPS, BDS, and GPS+BDS observations

Prediction of atmospheric corrections

Selecting the slant ionospheric delay calculated from the fixed RT PPP solutions as a reference, the accuracies of the interpolated satellite-differenced ionospheric delays for OUL2 are evaluated. Limited by the settings in the distance between reference and user stations, only three stations (KUU2, PYHA, TORN), of which the distances to the user station are about 170 km, 102 km, and 132 km, respectively, are applied for the interpolation. Due to limited space, we take the satellite pairs G24-G17 and C24-C18 as examples to show the predicted errors of the satellite-differenced ionospheric corrections in a continuous arc, and the results are plotted in Fig. 5. The performance of other satellite pairs during this period is similar. We can see that the predicted errors are smaller than 10 mm at most of the epochs, which suggests that the interpolation method works well in providing the ionospheric corrections for the rover users. Also, no obvious variation with satellite elevation exists and the performance of GPS and BDS satellites is similar.

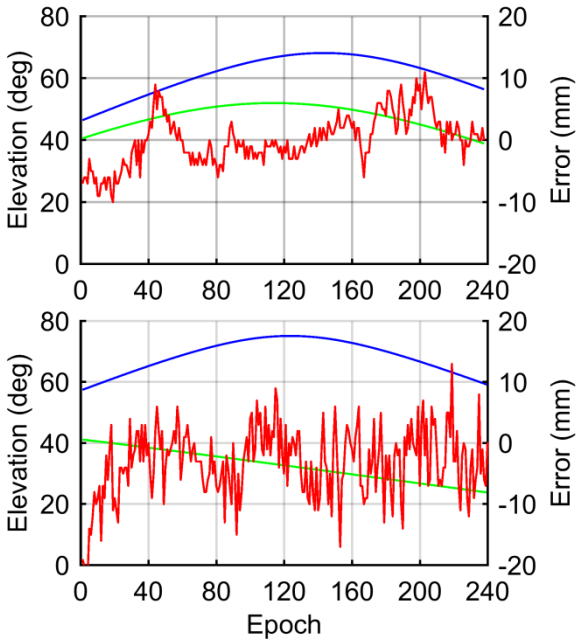

Fig. 5 Predicted ionospheric errors of G24-G17 (top) and C24-C18 (bottom) in a continuous arc. Blue and green lines represent the elevation of reference and roving satellite. Red lines represent the predicted ionospheric errors

Fig. 6 plots the RMS of the predicted satellite-differenced ionospheric information for station OUL2 at each epoch on DOY 358, 2018 obtained from GPS and BDS separately. The performance during the other two days is similar as illustrated in the figure. We can notice that the predicted accuracy of GPS and BDS are comparable, and the RMS of both systems is stable, except for an increase from UTC 6 to UTC 14. Except for a few epochs that are affected by bigger prediction errors for low elevation satellites, most of the RMS values are smaller than 6 cm, with mean RMS as 18.1 and 19.0 mm for GPS and BDS, respectively. The double-differenced (DD) slant ionospheric delays for a baseline length of 8.9 km can even reach magnitudes above 0.1 m when the Kp-index is 7- (Odolinski and Teunissen 2019), and in Europe may exceed half of the GPS L1 cycle length for a baseline length of 50-67 km when the Kp-index is 4o (Wielgosz 2011). Also as suggested in Wielgosz et al (2005), only 74.4% of the network derived DD ionospheric correction residuals are smaller than 10 cm, and the residuals can reach

up to 1 m in some cases during the day when the Kp-index reached 9o several times, and the distance between the reference and user station is 121 km. Compared with these previous results, the accuracies of the predicted ionospheric corrections in this analysis are better due to the calm ionospheric disturbance. It would become worse for medium and high ionospheric disturbance periods, as well as with the increasing distance between reference and user stations.

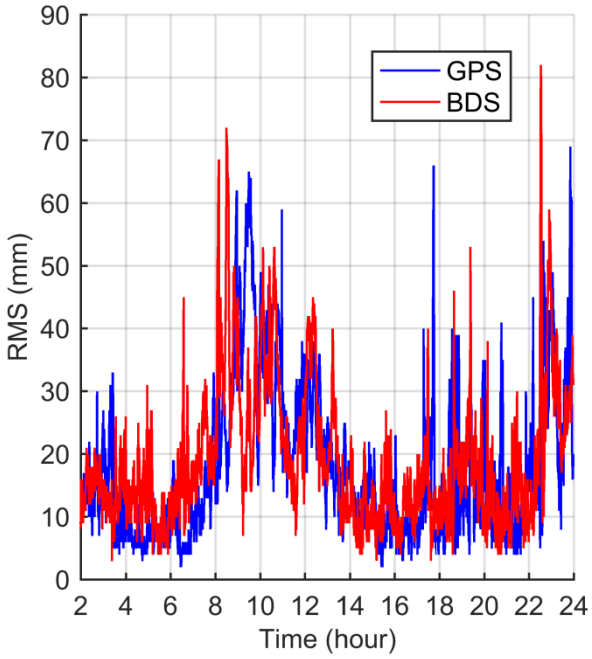

Fig. 6 RMS of predicted satellite-differenced ionospheric information at OUL2 on DOY 358, 2018

The predicted errors of the ZWDs compared with the results obtained from the fixed RT PPP solutions on DOY 358, 2018 are plotted in Fig. 7, and the performances during the other two days are also similar to this day. We can see that the predicted errors are smaller than 1 cm at nearly all epochs, and the RMS is 6.0 mm. By statistically evaluating the results of all three days, we find that the RMS of the predicted ionospheric information for GPS and BDS is 23.4 and 25.9 mm respectively, while the RMS of the predicted ZWDs is 5.6 mm. This accurately predicted atmospheric information provides a good basis for the following PPP-RTK.

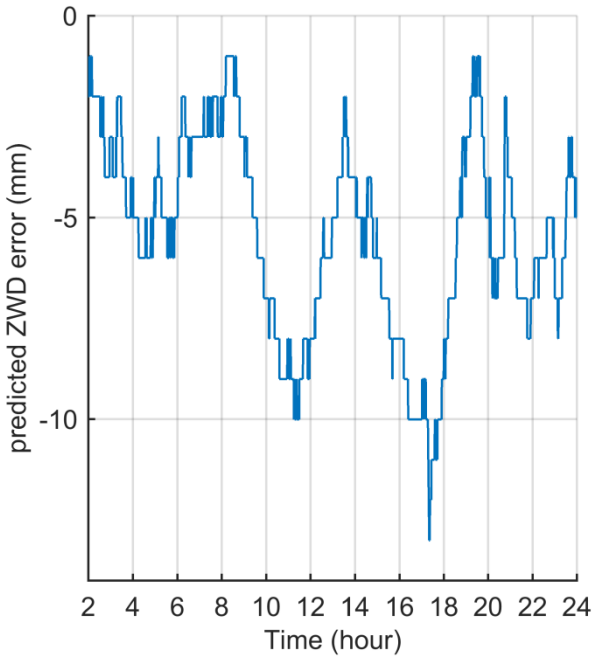

Fig. 7 Errors of predicted ZWD information at OUL2 on DOY 358, 2018

Performance of PPP-RTK

The observations are then processed every 3 minutes to evaluate the performance of PPP-RTK. Each time when the WL and NL ambiguities are both fixed successfully, and the positioning errors of the fixed solution are smaller than 4 cm and 10 cm for the horizontal and vertical components, respectively, we consider that the fixed solution has successfully been achieved. Fig. 8 shows the number of epochs applied to achieve the first fixed PPP solution and the number of NL ambiguities fixed for the solution on DOY 358, 2018, while the positioning errors of the fixed solutions are plotted in Fig. 9. The number of epochs is set to 7 if the fixed solution is not successfully achieved in the process.

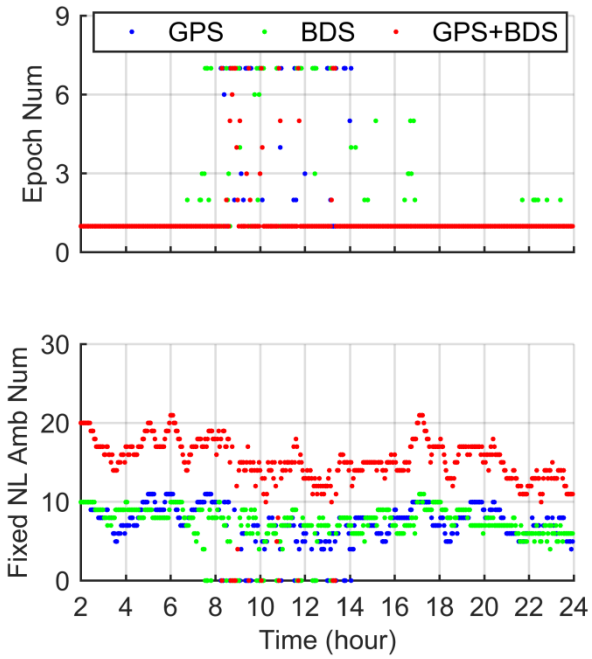

Fig. 8 Number of epochs required for the first fixed PPP solution (top) and the number of fixed NL ambiguities (bottom) based on observations of different satellite systems on DOY 358, 2018

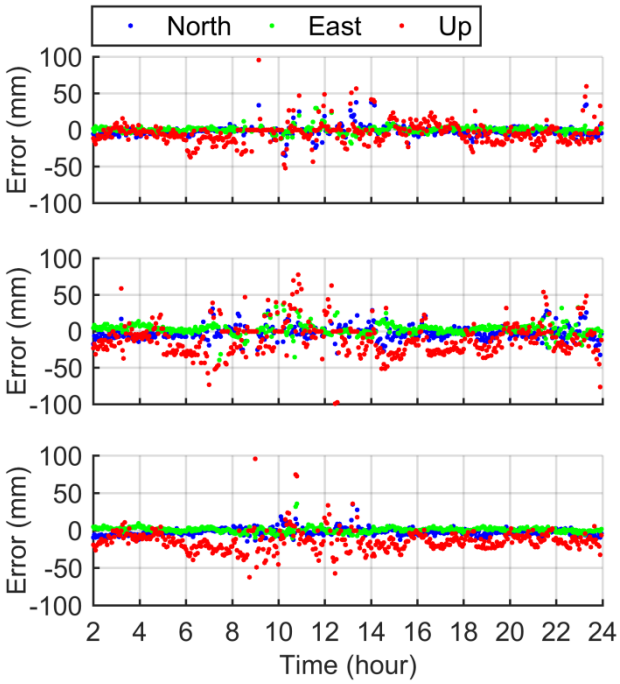

Fig. 9 Errors of the fixed solutions based on observations of different satellite systems on DOY 358, 2018. Top panel: GPS, middle panel: BDS, bottom panel: GPS+BDS

We find that the fixed solution can be successfully achieved based on

observations of one epoch in most processes when using single GPS or BDS observations, and the average number of epochs applied is 1.56 and 1.58, respectively (top panel, Fig. 8). We also notice that the number of fixed GPS and BDS NL ambiguities is comparable and varies between 5 and 10 most of the time, with average number as 7.0 and 7.1 for GPS and BDS, respectively (bottom panel). After ambiguity resolution, centimeter-level accuracy positioning results can be achieved for both systems. The RMS of the north, east and up components are 7.6, 4.4 and 15.4 mm respectively when using single GPS observation (top panel, Fig. 9), while 9.3, 8.2 and 25.1 mm if single BDS observations are used (middle panel).

The performance in PPP-RTK can be further improved by combining GPS and BDS observations (bottom panel, Fig. 9). This could be attributed to the improvement in the accuracy of float solutions and the number of ambiguity candidates. The average number of fixed NL ambiguities increases to 15.0, and the mean positioning accuracies of the fixed solutions, which can be achieved with an average of 1.2 epochs' observations, are 5.1, 3.8 and 19.8 mm respectively for the north, east and up components. The slightly worse positioning accuracy in the up component might be correlated to the weighting strategy between satellite systems in user positioning based on GPS+BDS observations, which requires further investigations.

The average number of epochs required to achieve the first fixed solution and the positioning accuracies of the fixed solutions during the analyzed three days are summarized in Table 1. We notice that centimeter-level positioning results can be achieved in less than 2 epochs on average based on single GPS or BDS observations, and the performance-based on single BDS observations is a little worse than that from single GPS observations. Positioning results with an accuracy of about 10 mm and 30 mm in horizontal and vertical directions can be achieved after an average of 1.6 epochs based on single BDS observations, while 9 mm in horizontal and 20 mm in vertical after an average of 1.5 epochs from single GPS observations. Such fixed solutions can be achieved after an average of 1.2 epochs when utilizing GPS and BDS observations together, and the positioning accuracies of the north, east and up components become 5.6, 3.5 and 23.3 mm respectively.

Our results are very encouraging, as it confirms that the BDS-3/BDS-2 system is now capable of providing high-accuracy positioning services, and the performance is close to GPS for users in Europe. In addition, the BDS observations can also contribute to shortening the time required to achieve the first fixed solution. Compared with single GPS observations, we notice that BDS could help improve the horizontal positioning accuracy based on GNSS observations. However, the vertical positioning accuracy becomes slightly worse when adding BDS observations to GPS, indicating that further researches in the weighting strategy between systems are still required to be conducted in the future.

As already revealed in Odolinski and Teunissen (2019), the TTFF is about 2 min for the high ionospheric disturbance period and can reach up to about 5 min when the Kp-index reaches up to 7- if using single frequency GPS+QZSS+BDS+Galileo observations due to the errors in the predicted ionospheric corrections. This value becomes about 1.5 min for dual-frequency GPS observations. Since our results confirm that BDS-3/BDS-2 observations are capable of providing high-accuracy positioning services comparable to other satellite systems, we anticipate that although the performance become worse, it would still be comparable as other satellite systems and could contribute to improving the performance of PPP-RTK when combining with other satellite systems during medium and high ionospheric disturbance periods.

Table 1 Statistical results on the performance of PPP-RTK based on observations from different satellite systems

System	Average Epoch	North (mm)	East (mm)	Up (mm)
GPS	1.5	8.0	4.7	19.7
BDS	1.6	9.8	7.3	29.7
GPS+BDS	1.2	5.6	3.5	23.3

Conclusions

The BDS system is now transiting from regional (Asia-Pacific) to global. In this study, the PPP-RTK based on BDS-3/BDS-2/GPS observations is realized, and its performance is evaluated in detail by utilizing the observations in Europe. Fixing the satellite orbits, we calculated the RT satellite clock offsets first, and then fixed to extract the UPDs and atmospheric information. RT PPP and PPP AR based on raw observations are realized at the user, and the ionospheric and tropospheric constraints predicted from the reference network stations, if available, are imported as virtual observations to realize PPP-RTK. Analysis results for three days reveals that centimeter-level accuracy positioning results can be achieved in RT PPP based on GPS or BDS only observations, and such performance can be further improved by realizing PPP AR and utilizing GPS/BDS observations together. The RMS of the fixed PPP solutions based on BDS+GPS observations reduce to 3.0, 2.0 and 8.8 mm in the north, east and up directions.

Based on the atmospheric information calculated from the network data processing at the server, interpolated ionospheric and tropospheric results with accuracy of 24.6 mm and 5.6 mm can be predicted for the users. Through importing the predicted atmospheric information as constraints, PPP-RTK positioning can be achieved in 1.5 and 1.6 epochs based on GPS or BDS only observations respectively. The RMS of the north, east, and up components are 8.0, 4.7 and 19.7 mm based on single GPS observations, while 9.8, 7.3 and 29.7 mm for BDS only observations, confirming that high-accuracy user positioning can be achieved based on BDS-3/BDS-2 only observations, and the performance is close to that based on GPS only observations. The PPP-RTK positioning can be further accelerated by utilizing GPS and BDS observations together, with an average number of 1.2 epochs, and the positioning RMS becomes 5.6, 3.5, and 23.3 mm for the north, east, and up components respectively. Our results suggest that BDS can now provide high accuracy positioning services alone for those users in Europe. In addition, although

there is a small decrease in the positioning accuracy for the vertical component, which might be attributed to inappropriate weighting strategy between satellite systems and requires further researches, the additional BDS observations can help shortening the time required to achieve the first fixed solution and also improve the positioning accuracies with respect to GPS only positioning. Finally, it must be stressed again that the ionospheric disturbance during the period analyzed is low, thus achieving a very good performance in PPP-RTK. Further analysis in the relationship between the ionospheric activity and the performance of PPP-RTK based on BDS-3/BDS-2/GPS observations is still required in the future to fully evaluate the effects of the BDS-3 observations in high-accuracy GNSS applications.

Acknowledgments

We thank the European Permanent GNSS Network (EPN) for providing the GNSS data. This research is supported by Hong Kong EC/RGC Collaboration Scheme (E-PolyU501/16) and The Research Institute for Sustainable Urban Development of Hong Kong Polytechnic University.

Reference

Bock H, Roof R, Yoon Y, Montenbruck O (2009) GPS clock correction estimation for near real-time orbit determination applications. Aerospace Science and Technology 13(7):415-422

Boehm J, Niell A, Tregoning P, Schuh H (2006) Global Mapping Function (GMF): A new empirical mapping function based on numerical weather model data. Geophys Res Lett 33(7), https://doi.org/10.1029/2005GL025546

de Haan S, Holleman I, Holtslag AAM (2009) Real-time water vapor maps from a

546 GPS surface network: Construction, validation, and applications. Journal of
547 Applied Meteorology and Climatology 48(7):1302-1316

548 Dai L, Han S, Wang J, Rizos C (2003) Comparison of interpolation algorithms in
549 network-based GPS techniques. Navigation 50(4):277-293

550 Defraigne P, Aerts W, Pottiaux E (2015) Monitoring of UTC (k)'s using PPP and IGS
551 real-time products. GPS Solut 19(1):165-172

552 Dong D, Bock Y (1989) Global positioning system network analysis with phase
553 ambiguity resolution applied to crustal deformation studies in California. J
554 Geophys Res 94(B4):3949-3966

555 Geng J, Shi C (2017) Rapid initialization of real-time PPP by resolving undifferenced
556 GPS and GLONASS ambiguities simultaneously. J Geod 91(4):361-374

557 Ge M, Gendt G, Rothacher M, Shi C, Liu J (2008) Resolution of GPS carrier-phase
558 ambiguities in Precise Point Positioning (PPP) with daily observations. J Geod
559 82(7):389-399

560 Ge M, Chen J, Douša J, Gendt G, Wickert J (2012) A computationally efficient
561 approach for estimating high-rate satellite clock corrections in realtime. GPS
562 Solut 16(1):9-17

563 Kamil K, Krzysztof S, Tomasz H (2018) Quality assessment of multi-GNSS orbits
564 and clocks for real-time precise point positioning. GPS Solut 22(11).
565 https://doi.org/10.1007/s10291-017-0678-6

566 Kouba J (2009) A guide to using international GNSS service (IGS) products.
567 ftp://ftp.igs.org/pub/resource/pubs/UsingIGSProductsVer21_cor.pdf

568 Laurichesse D, Mercier F, Berthias JP (2009) Real time precise GPS constellation
569 orbits and clocks estimation using zero-difference integer ambiguity fixing. Proc.
570 ION ITM 2009, Institute of Navigation, Anaheim, CA, USA, January 26-28,
571 664-672

572 Li X, Zhang X, Ge M (2011) Regional reference network augmented precise point

positioning for instantaneous ambiguity resolution. J Geod 85(3):151-158

Li X, Ge M, Dai X, Ren X, Fritsche M, Wickert J, Schuh H (2015) Accuracy and reliability of multi-GNSS real-time precise positioning: GPS, GLONASS, BeiDou, and Galileo. J Geod 89(6):607-635

Li X, Yuan Y, Zhu Y, Huang J, Wu J, Xiong Y, Zhang X, Li X (2019) Precise orbit determination for BDS3 experimental satellites using iGMAS and MGEX tracking networks. J Geod 93(1):103-117

Liu T, Yuan Y, Zhang B, Wang N, Tan B (2017) Multi-GNSS precise point positioning (MGPPP) using raw observations. J Geod 91(3):253-268

Lou Y, Gong X, Gu S, Zheng F, Feng Y (2017) Assessment of code bias variations of BDS triple-frequency signals and their impacts on ambiguity resolution for long baselines. GPS Solut 21(1):177-186

Montenbruck O, Hauschild A, Steigenberger P, Hugentobler U, Teunissen PJG, Nakamura S (2013) Initial assessment of the COMPASS/BeiDou-2 regional navigation satellite system. GPS Solut 17(2):211-222.

Nadarajah N, Khodabandeh A, Wang K, Choudhury M, Teunissen PJG (2018) Multi-GNSS PPP-RTK: From large- to small-scale networks. Sensors 18(4):1078. https://doi.org/10.3390/s18041078

Odijk D, Zhang B, Khodabandeh A, Odolinski R, Teunissen PJG (2016) On the estimability of parameters in undifferenced, uncombined GNSS network and PPP-RTK user models by means of S-system theory. J Geod 90(1):15-44

Odolinski R, Teunissen PJG, Odijk D (2013) Quality analysis of a combined COMPASS/BeiDou-2 and GPS RTK positioning model. International Global Navigation Satellite Systems Society (IGNSS) Symposium, Outrigger Gold Coast, Queensland, Australia, July 16-18, 2013

Odolinski R, Teunissen PJG (2019) An assessment of smartphone and low-cost multi-GNSS single-frequency RTK positioning for low, medium and high

ionospheric disturbance periods. J Geod 93(5):701-722

Pan Z, Chai H, Kong Y (2017) Integrating multi-GNSS to improve the performance of precise point positioning. Advances in Space Research 60(12): 2596-2606

Steigenberger P, Hugentobler U, Hauschild A, Montenbruck O (2013) Orbit and clock analysis of Compass GEO and IGSO satellites. J Geod 87(6):515-525

Tegedor J, Øvstedal O, Vigen E (2014) Precise orbit determination and point positioning using GPS, GLONASS, Galileo and BeiDou. Journal of Geodetic Science 4(1):65-73

Teunissen PJG (1995) The least-squares ambiguity decorrelation adjustment: a method for fast GPS integer ambiguity estimation. J Geod 70(1-2):65-82

Wanninger L, Beer S (2015) BeiDou satellite-induced code pseudorange variations: diagnosis and therapy. GPS Solut 19(4):639-648

Wielgosz P (2011) Quality assessment of GPS rapid static positioning with weighted ionospheric parameters in generalized least squares. GPS Solut 15(2):89-99

Wielgosz P, Kashani I, Grejner-Brzezinska D (2005) Analysis of long-range network RTK during a severe ionospheric storm. J Geod 79(9):524-531

Wübbena G, Schmitz M, Bagge A (2005) PPP-RTK: Precise Point Positioning Using State-Space Representation in RTK Networks. Proc. ION GNSS 2005, Institute of Navigation, Long Beach, CA, USA, September 13-16, 2584-2594

Xu X, Li M, Li W, Liu J (2018) Performance analysis of Beidou-2/Beidou-3e combined solution with emphasis on precise orbit determination and precise point positioning. Sensors 18(1):135. https://doi.org/10.3390/s18010135

Yan X, Huang G, Zhang Q, Liu C, Wang L, Qin Z (2019) Early analysis of precise orbit and clock offset determination for the satellites of the global BeiDou-3 system. Adv Space Res 63(3):1270-1279

Yang Y, Li J, Wang A, Xu J, He H, Guo H, Shen J, Dai X (2014) Preliminary assessment of the navigation and positioning performance of BeiDou regional

navigation satellite system. Sci China Earth Sci 57(1):144-152

Yang Y, Tang J, Montenbruck O (2017) Chinese navigation satellite systems. In: Teunissen, P., Montenbruck, O. (Eds.), Springer Handbook of Global Navigation Satellite Systems. Springer, Berlin, pp 273–304 (Chapter 10).

Yang Y, Xu Y, Li J, Yang C (2018) Progress and performance evaluation of BeiDou global navigation satellite system: Data analysis based on BDS-3 demonstration system. Sci China Earth Sci 61(5):614-624

Zhang B, Teunissen PJG, Odijk D (2011) A novel un-differenced PPP-RTK concept. J Navig 64(S1):S180-S191

Zhao Q, Wang C, Guo J, Wang B, Liu J (2018) Precise orbit and clock determination for BeiDou-3 experimental satellites with yaw attitude analysis. GPS Solut 22(4), https://doi.org/10.1007/s10291-017-0673-y

Zhang X, He X (2016) Performance analysis of triple-frequency ambiguity resolution with BeiDou observations. GPS Solut 20(2):269-281

Zhang X, Wu M, Liu W, Li X, Yu S, Lu C, Wickert J (2017) Initial assessment of the COMPASS/BeiDou-3: new-generation navigation signals. J Geod 91:1225-1240

Zhang R, Tu R, Liu J, Hong J, Fan L, Zhang P, Lu X (2018) Impact of BDS-3 experimental satellites to BDS-2: Service area, precise products, precise positioning. Adv Space Res 62(4):829-844

Author Biographies

Zhao Li is currently a research fellow at the Department of Land Surveying and

649 Geo-Informatics, Hong Kong Polytechnic University. She obtained her B.Sc.,
650 MSc and Ph.D. degrees in Geodesy at the School of Geodesy and Geomatics,
651 Wuhan University in 2006, 2008 and 2012. Her main research interests include
652 GNSS data processing and coordinate time series analysis.

653

654 **Wu Chen** is a Professor at the Department of Land Surveying and Geo-Informatics,
655 Hong Kong Polytechnic University. Prof Chen has been actively working on
656 GNSS related research for more than 30 years. His main research interests are the
657 GNSS positioning quality evaluation, system integrity, various GNSS applications,
658 seamless positioning, and SLAM.

659

660 **Rengui Ruan** is currently a research fellow at the Xi'an Research Institute of
661 Surveying and Mapping. He obtained his B.Sc., MSc and Ph.D. degrees at the
662 Engineering Information University in 2006, 2009 and 2018. His main research
663 interests include precise positioning, orbit determination, and time and frequency
664 transferring with GNSS.

665

666 **Xuexi Liu** is a Ph.D. candidate at the School of Geodesy and Geomatics, Wuhan
667 University. He received his B.Sc. degree from China University of Mining and
668 Technology in 2015. His current research mainly focuses on multi-GNSS precise

positioning and orbit determination.